Aerodynamic Characteristics of 2D Sail Sections

Abstract. The paper discusses the characteristics of 2D sail sections with optimal camber for different forms of the mean line. The influence of the mast is investigated. An envelope of the polar curves for the optimal shape is proposed.

NOMENCLATURE

AR	aspect ratio s/c
c	chord length, distance from luff to leach
C_D	drag-force / ($q \cdot c \cdot s$) parallel to U
C_L	lift-force / ($q \cdot c \cdot s$) vertical to U and span
C_p	pressure coefficient = $(p-p_\infty)/q$
D	long axis of elliptical mast profile
f	camber = maximum y-value of mean line
F	frequency of T.S. waves
H	height of wind tunnel vertical to U & span
N_{crit}	amplification factor in e^N -method
p	static pressure on model surface
p_∞	static pressure in undisturbed flow
q	dynamic pressure = $\rho/2 \cdot U^2$
Re	Reynolds-number = $U \cdot c/\nu$
s	span of tested profile section
t	maximum thickness of profile
TI	turbulence intensity $= \sqrt{\overline{u'^2}}/U$
u'	fluctuating part of velocity U
U	apparent wind speed far ahead of sail
x, y	coordinates parallel and vertical to chord
x_{ac}	distance of resultant lift force from luff
x_f	distance of max. camber f from luff
x_{tr}	distance of transition point from luff
α	angle of attack
α_{opti}	angle of attack at minimum C_D
β_{LE}, β_{TE}	angle of mean line at leading/ trailing edge
γ	sheeting angle
ρ	density of air = 1.225 kg/m^3 (stand. atm.)
ν	kinematic viscosity of air = $1.461 \cdot 10^{-5}$ m^2/s

1 INTRODUCTION

Part of the performance improvement of a sailing yacht is the optimization of all geometric dimensions of the sail plan. Classical wing theory [1] can be used to calculate the global lift- and drag-forces and to optimize the 3D-effects. These methods require as input the aerodynamic characteristics of the 2D sail sections at a large number of stations between deck and masthead. For profiled wing sections as they are used on airplanes but also for yacht keels, there is the well-known reference book by Abbott & Doenhoff [2]. Such a systematic analysis does not exist for sails, which are characterized by very thin and highly cambered sections.

The aerodynamic properties of 2D sections were first measured in wind tunnels and are more lately predicted by computer simulations. Maughmer and Coder [3] compared measurements on airfoils in the Penn State University Low-Turbulence Wind Tunnel to the predictions of several codes, including state of the art CFD programs. They concluded that: “In general, the drag predictions of the codes incorporating boundary-layer methods generally agreed better with the experimental results than did those of the Navier-Stokes solvers, while all of the theoretical methods generally over-predicted the maximum lift coefficient”. They stated that: “- reasonably accurate viscous pressure distributions, which capture the influence of limited trailing-edge separation and laminar separation bubbles, are predicted” by XFOIL [4]. For sails with thin and highly cambered sections, which always suffer from a separation bubble at the leading edge and exhibit also early separation on the suction side, XFOIL seems to be the method of choice. Comparisons of the predictions with the wind tunnel measurements that are presented in the following chapter, verify this statement. The C_P-distribution matches the experimental results quite well in the medium α range around the ideal angle of attack and hence the lift coefficient C_L is also acceptable. The drag coefficient C_D is on the contrary massively underpredicted. This is most likely caused by the very thin leading edge, which causes extremely high velocities and a suction peak. In the real flow, there will be a separation bubble and the suction force, that reduces the overall drag, will not be present. Since the 3D wing codes [1] need the polar curves of drag vs. lift as input, accurate experimental results should be preferable to the computer predictions. In the next chapter, we will investigate experimental results for the flow around headsails without a mast in windward sailing.

2 EXPERIMENTAL RESULTS IN THE LITERATURE

2.1 Similarity rules

For the selection of suitable experimental results, it is essential to know the values of the dimensionless parameters that guarantee the similarity between the flow in the wind tunnel and the sail at full size. The

following table lists the different parameter ranges that occur when sailing different yachts in different conditions. The relative thickness *t/c* includes the leading (L.E.) and trailing edges (T.E.). The sailcloth itself is very thin, but the edges are thicker because of the boltrope. The thickness of the L.E. increases further, if the forestay carries a profiled aluminum luff extrusion. These thicknesses at the edges determine the flow and not the thickness of the cloth. Since the chord decreases from the foot to the head of the sail, *t/c* and Reynolds-number vary. The numbers in the table are representative for the geometric center of the sail. The indicated range of Reynolds-numbers covers all the condition from a small boat with a sail-chord of 1 meter sailing in a 3 kts. wind at the low end up to a large yacht in Bft. 8 with a 6 meter sail-chord.

camber *f/c*	*t/c* boltrope	*t/c* luff extrusion	Reynolds-number *Re*	turbulence intensity *TI*
7% – 20%	0.2%	0.6% – 0.8%	$1.6 \cdot 10^5 - 9 \cdot 10^6$	1.5% + bypass transition

Turbulence intensity is the relation between the standard deviation of the turbulent velocity fluctuations and the speed of the onset flow. Its level determines the transition point from laminar to turbulent flow. Airplanes flying at high speed at very low turbulence levels use airfoils with a favorable pressure gradient along a large part of the chord and achieve extended laminar flow. This reduces significantly the drag at the design angle of attack [2]. Compared to airplanes, sails operate at very low speeds in the highly turbulent atmospheric boundary layer. Weiler & Burling [5] measured spectra of the velocity fluctuations in a distance of two to three meters above the sea surface and at wind speeds between 3 and 20 knots. The fluctuations are very high at low frequencies and decrease towards the higher frequencies. The linear stability theory that explains the natural transition of the boundary layer is based on the occurrence of Tollmien-Schlichting (T.S.) waves. The frequencies that cause instability were measured [6] and can be calculated. The highest *TI* occurs at the lowest frequency that causes transition. This frequency *F* is a function of the apparent wind speed:

$$F = \frac{1.8 \cdot 10^{-6}}{\nu} \cdot U^2 \qquad \text{(Hz)} \tag{1}$$

Assuming boat speeds between 2 and 13 knots, matching the given wind speeds, the turbulence intensity that can cause natural transition follows from the measured spectra. Values between 1% and 1.5% can be expected in the given range of wind- and boat speeds. Flay and Jackson [7] arrive with similar calculations at a formula, that results in *TI* = 2.4% upwind. The very high turbulence at low frequencies will not be able to cause T.S.-waves, but it has an impact. In recent years, the wind turbine industry started the research on this subject, because a reduction in profile drag would significantly improve the efficiency of wind turbines. Field studies near the sea shore [8],[9] locating the transition point on the blade with hot film sensors revealed, that the high turbulence level in the atmospheric boundary layer caused early bypass transition and laminar flow was almost inexistent. Since sails move at slower speeds than the rotating blades of a wind turbine, the turbulence level on sails will be even higher and bypass transition will occur, before T.S. waves are generated. Laminar flow around sails is most likely not possible. The test in a wind tunnel can be misleading under such circumstances, because the flow in the wind tunnel has usually a much lower turbulence level.

2.2 Review of the experimental data for circular arc profiles of 10% camber

All the experimental data of thin airfoils in the open literature are, with two exceptions, about circular arc profiles. For sections with a camber of 10%, the results from four different authors can be compared. The polar

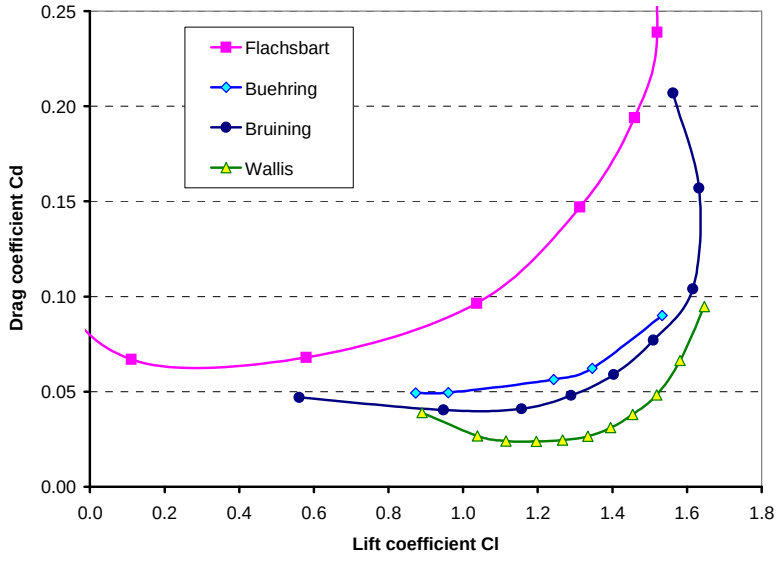

Figure 1. Polar curves for circular arcs with 10% camber, L.E. and T.E. rounded

Author	Reynolds-number	*TI*	*t/c*	aspect ratio	*c/H*	drag measured
Flachsbart [10]	$4.1 \cdot 10^5$	0.24%	1.5%	5	0.09	w/balance
Buehring [11]	$3.4 \cdot 10^5$	<0.5%	0.64%	4.8, with false walls ?	0.21	w/balance
Bruining [12]	$3.5 \cdot 10^5$	0.02%	2%	5, end plate + false wall	0.08	w/balance
Wallis [13]	$3.1 \cdot 10^5$	0.6%	2.1%	4, with end plates	0.07	wake pressure

curves are shown in figure 1 and the model- and tunnel parameters are listed in the table above. The raw data from the wind tunnel must be corrected for the influence of the tunnel walls [14]. Only Bruining applied some corrections to his data. Buehring discussed the tunnel interference in detail, but decided at the end to ignore it and published the uncorrected data. Because his ratio of chord to tunnel height (*c/H*) is not small, his results should be corrected for blockage, streamline curvature and separated flow [14]. The data points of Buehring's curve in figure 1 have been corrected.

It is obvious that Flachsbart's measurements stick out. He measured a rectangular wing of aspect ration 5 in an open jet. The measured values were then extrapolated to 2D-flow of infinite aspect ratio. The rules for extrapolation are valid for normal wings with attached flow and a lift slope close to the theoretical value of 2π. These rules are not applicable to a thin and cambered arc with a separation bubble at the L.E. and massive separation at the rear of the airfoil. In the year 1932 a better method was not yet available.

The other authors approximated 2D-flow by placing a finite span of the airfoil between reflection planes, but to achieve a truly 2D-flow with separation is not an easy task [15], [16]. Depending on the geometry of the airfoil and on the thickness of the wall boundary layer, the flow close to the walls can be separated, while the flow at the center of the airfoil is still attached [15] or vice versa [16]. Therefore the drag should be determined from pressure measurements, traversing at the centerline in the wake. Balance measurements of the drag are not accurate, because the balance will measure an average value along the span of the 3D-mixture of separated and attached flow. To avoid the thick boundary layers at the tunnel walls, the authors placed the airfoils between end plates or false walls. The problem with end plates is that they are never large enough to eliminate the flow around the tips [15]. False walls avoid this, because they extend to the walls that run parallel to the airfoil. Buehring calls his devices "end plates", but comparing his test results of sailwings that extended to the tunnel walls with the similar values of the circular arc, one must conclude, that he used false walls.

None of the available wind tunnel tests fulfills the requirements for accurate 2D-flow. Buehring's test setup has the closest proximity to the similarity parameters of sails. The correct thickness seems to be crucial, since the suction peak and the separation bubble will increase, when the thickness decrease. The higher drag in Buehring's experiment compared to Bruining's qualitatively similar results must be caused by the reduced thickness. The lower drag measured by Wallis for experimental conditions that are almost identical to Bruining's could be attributed to the fact, that Wallis deduced the drag from wake traverses, compared to Bruining's use of a balance. A more likely reason could be Wallis' higher turbulence intensity, because a turbulent boundary layer will start to separate at a much higher angle of attack than a laminar b.l. This would explain the lower drag above $C_L = 0.9$.

Buehring tested his airfoils also at different Reynolds-numbers. The results for $Re = 1.2 \cdot 10^5$ and $1.7 \cdot 10^5$ are quite similar, also similar are the curves for $Re = 2.5 \cdot 10^5$ and $3.4 \cdot 10^5$. Between these two groups, there is a jump of C_L at the optimal angle of attack from 0.9 to 1.2. At $Re = 2 \cdot 10^5$ the flow obviously changes its character. This phenomenon was investigated in [17] for a sail model with 30% camber. The authors found out, that at the lower Reynolds-numbers the flow on the suction side remains laminar and the boundary layer separates before the flow becomes turbulent. At the higher Reynolds-numbers the boundary-layer transitions to turbulent flow and stays attached further towards the T.E. on the suction side. The attached flow produces a higher lift coefficient. The authors recommend to run experiments at Reynolds-numbers above $Re = 2.3 \cdot 10^5$ to avoid laminar separation, which has no equivalence in the flow around full-size sails. The root cause is the far too low turbulence intensity in the wind tunnel, which makes the necessary bypass transition impossible, as was already discussed in the chapter about the similarity rules.

2.3 Experimental data for circular arc profiles of optimal camber

Buehring [11] tested profiles of 7.1% to 12.5%. For higher camber there are the experiments by Milgram [18] and Bot [19]. Experiments by Chapleo (referenced in [20]) are limited to Reynolds-numbers below $Re = 2 \cdot 10^5$

and are therefore not applicable. Milgram tested airfoils from 12% to 18% camber with NACA 65 mean lines, which are identical to circular arcs. He explains in detail his data reduction process and writes, "It should be noted here that wall effects have been neglected in the data reduction". To make his results comparable they are corrected for blockage and streamline curvature. Because of the extremely high *c/H*-value, Maskell's wake blockage correction for separated flow [14] is applied. Milgram performed his tests in a circulating water tunnel with unknown turbulence intensity. Bot tested a circular arc of 20.3% camber also in a water tunnel. Bot lists a higher camber in his paper, but in the usual definition [2] the camber refers to the mean line. His results also had to be corrected in the same manner as Milgram's. The polar curves are depicted in figure 2 and the model- and tunnel parameters are listed in the following table.

Author	Reynolds-number	*t/c max*	*t/c at LE,TE*	aspect ratio	*c/H*
Buehring [11]	$3.4 \cdot 10^5$	0.64%	0.64%	4.8, with false walls	0.21
Milgram [18]	$6 \cdot 10^5$	3.44%	0.22%	2.2, between walls	0.46
Bot [19]	$3.69 \cdot 10^5$	4.0%	48° wedge	2.6, between walls	0.39

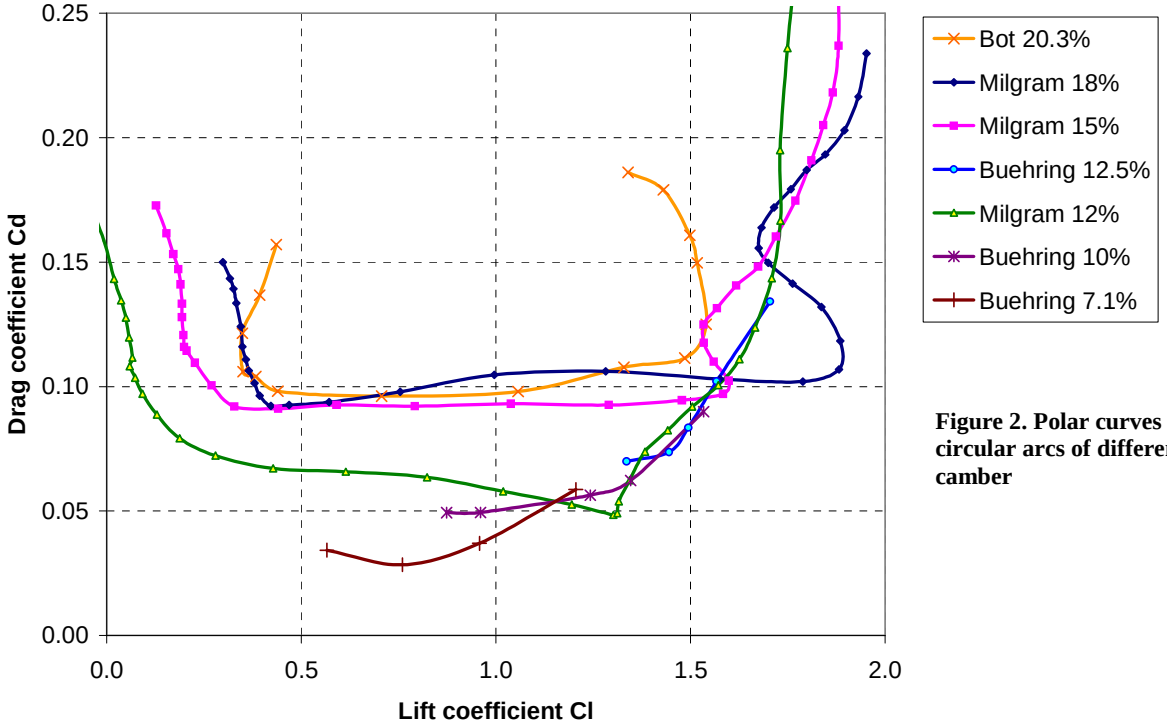

Figure 2. Polar curves for circular arcs of different camber

All three authors measured the forces with a balance. As described, this method introduces an error that increases with decreasing aspect ratio. van den Berg [15] reports experimental evidence for severe errors at an aspect ratio of 3.5 at full stall. Results with aspect ratios below 4 are generally questionable. The ratio *c/H* must be less than 0.3 according to van den Berg. Milgram and Bot violate the requirements for aspect ratio as well as tunnel height. Looking at the polar curves in figure 2, Milgram's result for 18% camber stands out. It is questionable, whether real sails can achieve the high C_L-values, which he measured. The highest 2D-C_L-value that the ORC [21] uses in its VPP is C_L=1.7 for highly cambered headsails set flying (e.g. code0). This value would fit well with all polar curves in figure 2, except Milgram's for 18%. Maskell proposes in his correction for separated flow [14] also an increase in the effective dynamic pressure because of the blockage effect of the flow separation. This would result in a lower corrected lift coefficient. Since this correction requires the base pressure, which is unknown in Milgram's case, the additional correction could not be applied. This might explain his high C_L-values.

An envelope through the points with the highest C_L/C_D-ratios will form the polar curve for the circular arc profiles with optimal camber. Figure 3 shows a smoothed curve that is the best guess for this optimum. The flat plate was only added to the diagram to show the asymptotic limit, it is of course not suited for a sail. Equation 2 will give the optimal camber, if the desired C_L is inserted. If the resulting camber is larger than 18%, the value for C_L is too high and cannot be realized.

$$f/c = 0.04783 \cdot C_L^{\,3} - 0.1035 \cdot C_L^{\,2} + 0.13666 \cdot C_L \qquad \leq 0.18 \tag{2}$$

The corresponding angles of attack and the position of the aerodynamic center would also be of interest. No smooth curves can be given, because there is no gradual shift in the flow, instead different cambers create significantly different flow regimes. For the angle of attack a very rough estimate can be calculated from equation 3:

$$\alpha = 2.238 \cdot C_L - 1.061 \qquad \alpha \text{ in degrees} \tag{3}$$

The position of the aerodynamic center x_{AC}/c varies between 0.455 and 0.495. It is close to the position of the maximum camber at x/c =0.5.

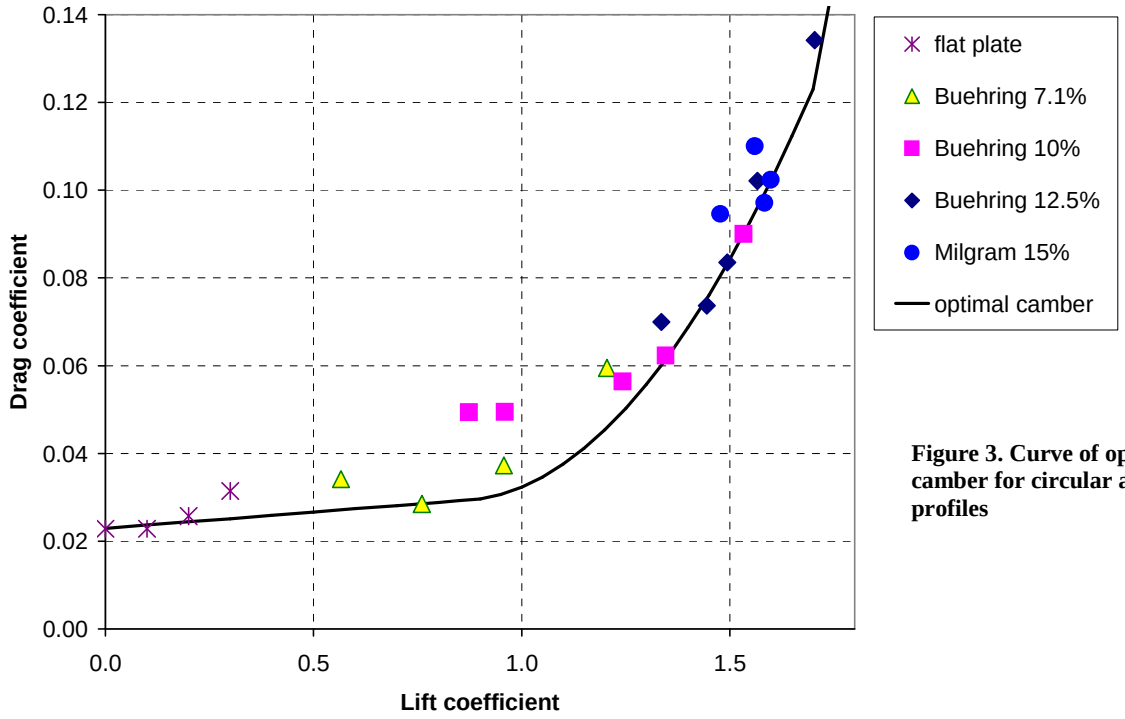

Figure 3. Curve of optimal camber for circular arc profiles

3 THE BEST PROFILE FOR SAILS

Sailing close-hauled to windward, the circular arc is not the best choice for the profile of sails. To investigate possible improvements one must have a tool that determines the polar curve from the geometry and the flow conditions. The previous chapter demonstrated the difficulties in getting reliable experimental data. A numerical prediction would be more flexible and truly 2-D, but the shortcomings of the computer program XFOIL were already mentioned. A solution could be the development of a correction that, when applied to the XFOIL-drag-coefficients, results in more realistic drag values. In the next chapter I will try this.

3.1 A modification to XFOIL

The drag values for thin sails, as predicted by XFOIL, are generally too low. The suction peak at the L.E. will not be present in reality and the suction force is overestimated. The suction force is proportional to $C_L \cdot \alpha$. In addition, the drag in the separated zone at the rear of the airfoil is obviously underestimated. One can assume that the separation drag will increase with increasing trailing edge angle β_{TE}. These assumptions lead to a correction for the measured C_D that sums up as shown equation 4:

$$C_D = C_{D,xfoil} + A \cdot (\alpha - \alpha_{opti}) \cdot C_L + 0.11236 \cdot \tan\beta_{TE} - 0.01229 \qquad \Delta\alpha \cdot C_L > -0.03 \quad \alpha \text{ in rad} \tag{4}$$

$$A = 3.824 \cdot \tan^2\beta_{LE} - 3.8762 \cdot \tan\beta_{LE} + 1.0342 \qquad 0.28 < \tan\beta_{LE} \leq 0.507$$

$$\tan\beta_{LE} = \frac{y_{2\%c} - y_{0\%c}}{0.02 \cdot c} \qquad \tan\beta_{TE} = \frac{y_{98\%c} - y_{100\%c}}{0.02 \cdot c} \qquad \text{mean line}$$

In thin airfoil theory the suction peak vanishes, when the airfoil is set at the ideal angle of attack and the flow is parallel to the mean line at the leading edge. In the real viscous flow around a highly cambered airfoil, the flow separates even at the ideal angle of attack and the flow does not follow the mean line at the L.E. An optimum angle of attack replaces therefore the ideal angle of attack in equation 4. α_{opti} is defined as the angle where C_D as predicted by XFOIL is minimal. The factor A, which modifies the correction for the suction forces, is not constant. A dependence on the L.E.- angle β_{LE} is assumed. Buehring's experimental data was used to determine the numerical values in equation 4, which is therefore only valid for the parameter range of his experiments. The modified XFOIL-polar-curves are depicted in figure 4 together with the experimental values.

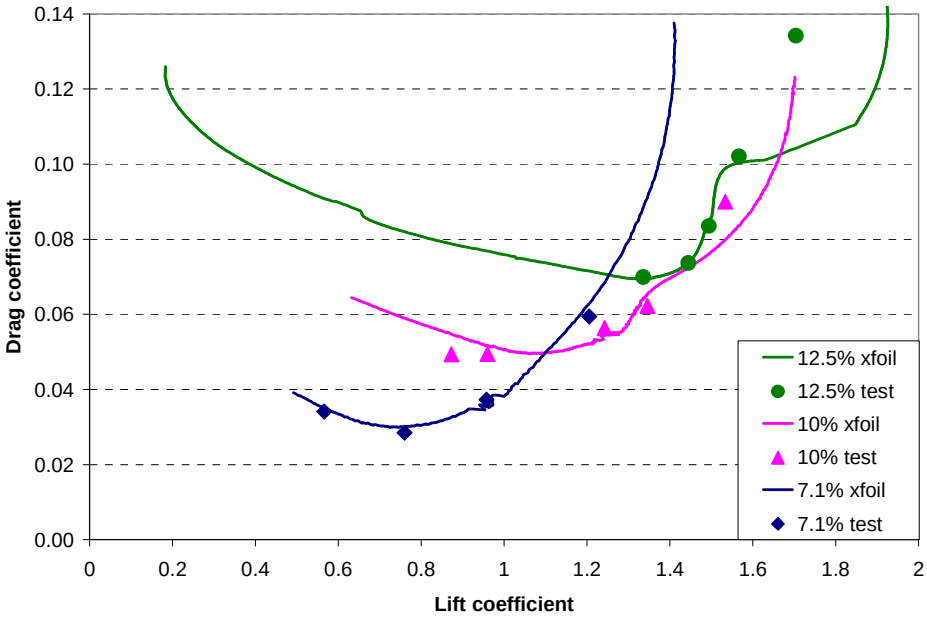

Figure 4. modified XFOIL-results compared to Buehring's circular arc data for different camber, Re = $3.4 \cdot 10^5$

It can be seen, that the prediction deteriorates, when the camber increases. For the determination of the optimal camber only the points at the highest lift/drag-ratio are of interest. In these areas the prediction of the modified XFOIL method is acceptable. Even if one does not want to trust the absolute values of the modified method, it is possible to use it for a comparison of different designs and identify the relatively better solution. It is important to remember, that the modification was developed for sails with a leading edge thickness of less than 1%. The factor A reduces to zero for a thicknesses $\geq$ 2%.

3.2 The optimum sail shape

Several authors [e.g. 20] investigated in a wind tunnel the shape of flexible 2-D membranes that are fixed only at the L.E and T.E. and are free to move in between. The length of the cloth relative to the chord length determines the maximum camber. The position of the maximum camber moves forward, as the angle of attack increases. This model with unrestricted sides has an additional degree of freedom that 3-D sails do not have. Modern sails are made of materials with high resistance to stretch. When the three sides of a triangular sail (luff, leech, foot) are fixed, the distribution of the camber is also fixed, independently of the angle of attack. The sailmaker determines the camber and its position, when he cuts and sews the panels of the sail. The sail trimmer can modify the camber and its distribution by changing the position and the tension of the three sides of the sail. Compared to this presetting, the wind forces will have only a minor influence on the shape of the sail. It is appropriate, to assume total outside control over the shape, when looking for optimal sail profiles. Therefore, most models in experimental work on 2-D sails consist of stiff materials, e.g. sheet metal. Another way to look at the problem is the identification of the stiff model as the flying shape of the sail. It is then up to the sailmaker and trimmer to achieve this flying shape by whatever means.

The two authors who published experimental results for thin and cambered airfoils that are not circular arcs are Lyon et al. [22] and Milgram [18]. Lyon et al. re-measured an old profile from Göttingen: Gö 417a. They used it as a benchmark for small wind turbines. The airfoil has a thickness of 3% and 5.8% max. camber, 38% behind the L.E. The position of the maximum camber seems favorable, but the thickness is too large and the camber too small to apply this profile to a sail. Milgram tested the NACA mean line a = 0.8. This mean line was designed for airfoils with extended laminar flow ("laminar bucket") [2] for the price of a steep pressure rise at the rear. The pressure rise will cause flow separation if the camber of the foil is high as with sails. In addition, the

constant pressure over 80% of the foil, which was intended to keep the flow laminar, is meaningless for sails. Because of bypass transition, laminar flow is not possible. The rear part of the profile has a concave curvature. This is impossible for flexible sails.

The best profile for sails on a close-hauled upwind course would allow high camber for high lift coefficients, but without separation of the boundary layer. To strive for this goal, a L.E. without extreme pressure spikes and a very gentle pressure rise on the suction side would be required. The NACA mean line $a = 0.1$ comes close to this ideal. Inviscid potential flow predicts a constant pressure for the first 10% of the chord [2]. This allows the flow to reattach, if there is a separation bubble at the sharp leading edge. For the rest of the chord the pressure on the suction side rises as gradual as possible up to the T.E., avoiding separation as long as possible. Unfortunately, the original mean NACA line cannot be applied to sails, because the curvature changes its sign in the rear part of the foil. A sail must be continually convex because the pressure difference between the pressure and suction side pushes the cloth always towards the suction side. A modified mean line is therefore proposed. A slightly convex mean line replaces the concave part of the foil in the rear. Figure 5 shows the C_P-distribution for this mean line as calculated with XFOIL and compares it to a circular arc. The XFOIL prediction uses the following sail model and flow parameters:

L.E. ellipse with	$t/c = 0.7\%$	position of max. camber:	
T.E. circle with	$t/c = 0.2\%$	- NACA $a = 0.1$ mod.	$x_f/c = 32\%$
sail cloth with	$t/c = 0.05\%$	- circular arc	$x_f/c = 50\%$
max. camber	$f/c = 12\%$	amplification factor	$N_{crit} = 0.5$
Reynolds-number	$Re = 4 \cdot 10^5$	transition point	$x_{tr}/c = 0.01$

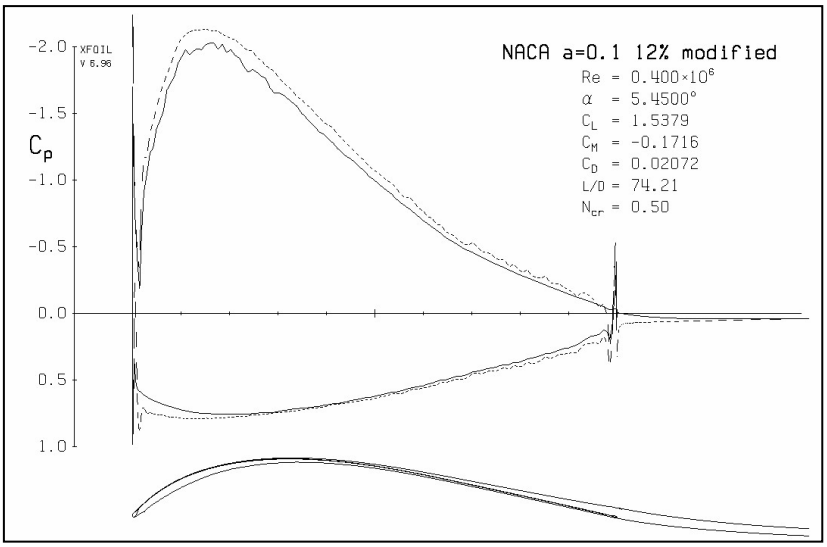

Figure 5a. pressure coefficient at maximum L/D-ratio for modified NACA $a = 0.1$

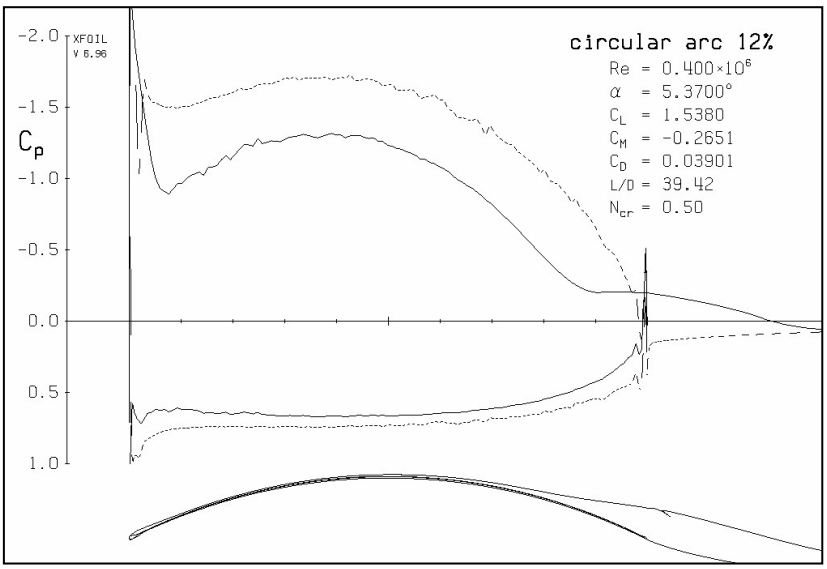

Figure 5b. pressure coefficient at equal lift for circular arc

The user's manual for XFOIL recommends "mimicking" bypass transition by setting N_{crit} to a value of less than 1 and additionally to set trips. Here x_{tr}/c = 0.01 was chosen as the latest transition point. Özçakmak et al. [9] made similar choices and modelled successfully the transition on rotor blades in free air.

The comparison between the two mean lines is made for identical lift coefficients. It is obvious that the larger T.E.-angle and hence the much steeper pressure gradient of the circular arc airfoil provokes massive flow separation and a negative base pressure. The newly proposed mean line has in comparison an attached flow up to the T.E. XFOIL predicts a rather thick boundary layer, but no separation, as the pressure coefficient at the T.E. reaches zero. There is a small dead-water zone behind the L.E., but this does not hurt the creation of lift. As a result, the lift to drag ratio of the new mean line is much better than that of the circular arc. Figure 6 shows the polar curves for the two sail sections with the two different mean lines, but identical thickness distribution.

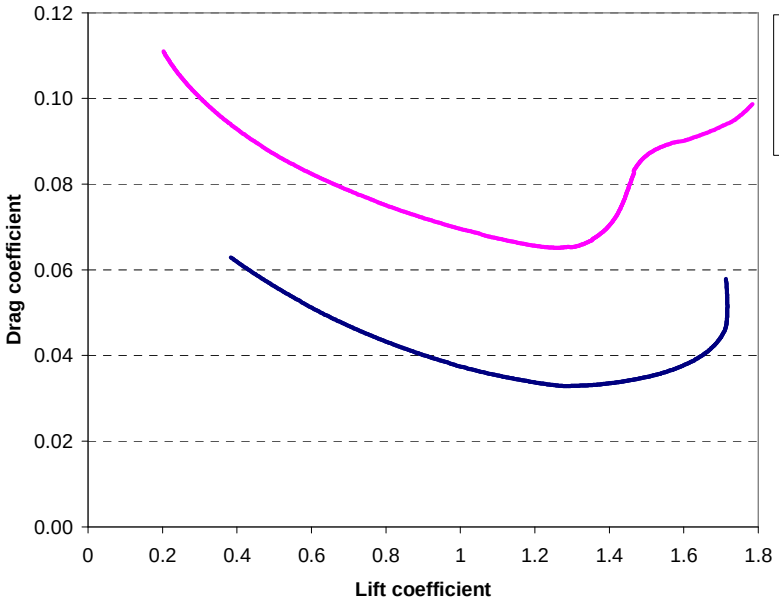

Figure 6. polar curves for sails with different mean lines, XFOIL predictions corrected as in eq. 4

3.3 The envelope for optimal camber

Just as for the circular arc in chapter 2.3, it is possible to collect all polar curves in one diagram and to draw an envelope that is tangent to all individual polar curves. This envelope connects the points of maximum lift to drag ratio for a given lift coefficient. Figure 7 shows the result for the new mean line *a = 0.1 – modified*.

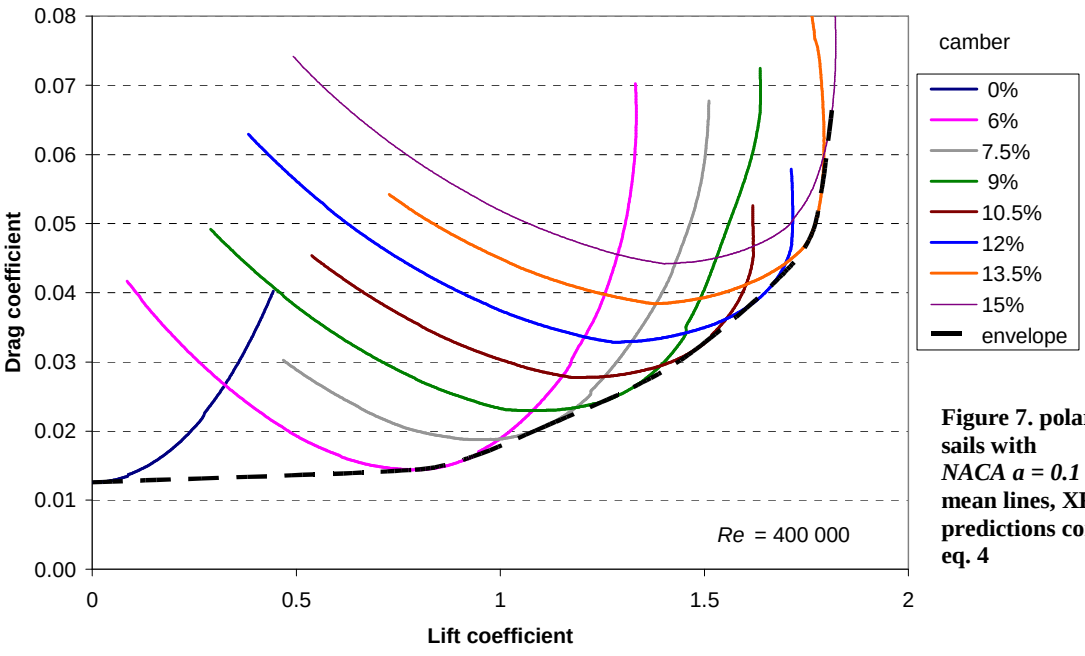

Figure 7. polar curves for sails with *NACA a = 0.1 modified* mean lines, XFOIL predictions corrected as in eq. 4

The envelope varies with the Reynolds-number. If the procedure that is illustrated in figure 7 is applied to the range of the relevant Reynolds-numbers, the result is a family of curves as depicted in figure 8. Linear interpolation is possible, if log(*Re*) is used.

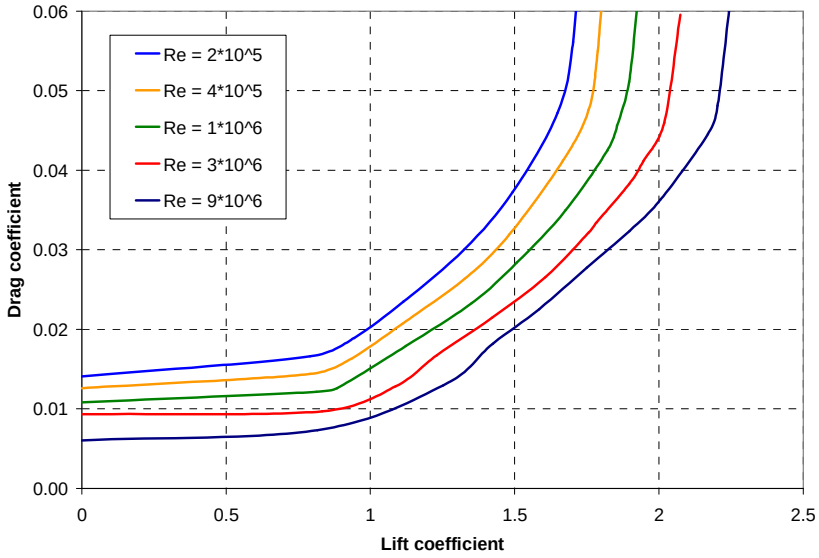

Figure 8. envelopes for sails with *NACA a = 0.1 modified* for different Reynolds-numbers

The corresponding optimal camber can be taken from figure 9. It is possible to determine an interpolating function for the angle of attack that is required to achieve the prescribed lift coefficient. Equation 5 exhibits the function and the calculation of the parameters. The base of the logarithm is 10 and $2 \cdot 10^5 \le Re \le 9 \cdot 10^6$.

$$\alpha = a \cdot C_L{}^2 + b \cdot C_L$$

$$a = \left\langle \begin{matrix} 0.0821 \cdot \log Re - 0.0862 \\ -0.1637 \cdot \log^2 Re + 1.1942 \cdot \log Re - 1.1759 \end{matrix} \right\rangle \left\langle \begin{matrix} \log Re \le 5.6061 \\ \log Re > 5.6061 \end{matrix} \right\rangle \qquad \alpha \text{ in degrees} \qquad (5)$$

$$b = 1.2978 \cdot \log^2 Re - 14.384 \cdot \log Re + 43.514$$

In the same way, equation 6 gives the interpolating function for the position of the aerodynamic center.

$$\frac{x_{AC}}{c} = d \cdot C_L + e$$

$$d = \left\langle \begin{matrix} -0.0134 \cdot \log^2 Re + 0.1475 \cdot \log Re - 0.3984 \\ 0.0323 \cdot \log Re - 0.1899 \end{matrix} \right\rangle \left\langle \begin{matrix} \log Re \le 6.007 \\ \log Re > 6.007 \end{matrix} \right\rangle \qquad (6)$$

$$e = -0.0422 \cdot \log^2 Re + 0.4806 \cdot \log Re - 1.0245$$

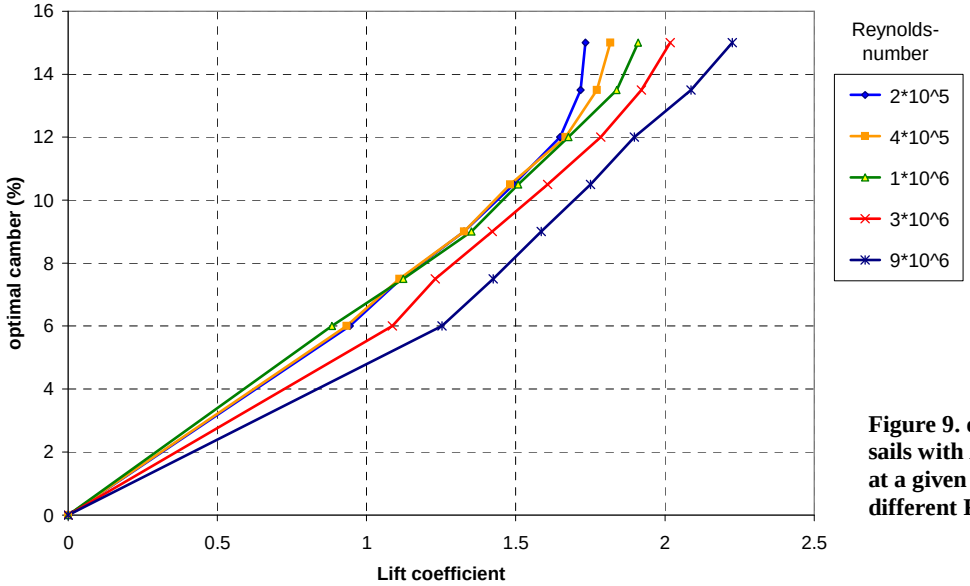

Figure 9. optimal camber for sails with *NACA a = 0.1 modified* at a given lift coefficient for different Reynolds-numbers

4 SAIL WITH MAST

If the sail is set behind a mast, the flow over the sail changes significantly its character. For every possible trim, there are large areas where the flow separates from the sail. Wilkinson [23] analyzed this in detail and measured the pressure and boundary-layer parameters on a 2D-sail-model in the wind tunnel. For the design and optimization of sail and mast, we need a computer program that can reliably predict the aerodynamic characteristics. Several authors proposed different CFD-tools and compared the results with Wilkinson's experimental data. Chapin et al. [24], using Ansys Fluent, conclude that "RANS simulations are able to qualitatively capture the main flow features of the mast-sail aerodynamic". Quantitatively the prediction is not sufficient. Renzsch [25] compared his results, obtained with Ansys CFX, as well as the results of two other authors to Wilkinson's data and drew a similar conclusion. He writes: "The difficulties in predicting spontaneous flow separation on a curved surface using RANS methods are well documented in literature and an ongoing topic of research". The creation of a database for the aerodynamic characteristics of all possible mast-sail combinations requires the variation of 5 parameters: sail camber, mast diameter, sheeting angle, angle of attack and Reynolds-number. To do this with a CFD-tool would impose a workload that is prohibitive. If the results achieved with CFD are not fully satisfactory, we might as well try to predict the flow with XFOIL that is fast and easy to run.

4.1 The independent parameters and their range

The independent parameters of the XFOIL-prediction for a given profile family for the headsail were the camber *f/c*, the angle of attack α and the Reynolds-number. With the addition of the mast, the mast diameter *D/c* and the sheeting angle γ are needed for the geometric description. The definition of these parameters can be taken from figure 10. To make the force coefficients comparable with the headsail, the definition of the chord length is still the distance between luff and leach of the sailcloth; the mast is not included. The mast cross section is modeled as an ellipse with the length of the small axis equal to $0.6 \cdot D$. During actual sailing on all courses, γ varies between 0° and almost 90°. A statistical survey of *D/c* for production boats at the boom level gave a minimum of 2.7% and a maximum of 5.6% for the larger and/or older yachts. Since the chord decreases towards the mast top, whereas *D* remains mostly unchanged, the parameter *D/c* needs to cover a range of 2.7% – 30% in the database. For the last part at the top of the mainsail the data can be extrapolated.

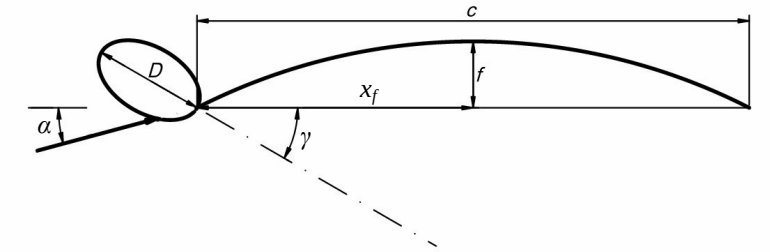

Figure 10. Definition of the geometric parameters

4.2 The XFOIL performance

To test the capabilities of XFOIL for these highly complex separated flows, we need reliable experimental data. In Wilkinson's experimental setup [23] his model consisted of flat and stiff bars with a width of 3% of the chord, that were connected by rubber joints. L.E. and T.E. were machined from flat elements with 7% width. The profile of the sail was approximated by deflecting the mat of flat bars at the rubber joints. In this way the curve of the profile is continuous, but the resulting curve is not differentiable at the joints. The curvature is therefore discontinuous and displays a series of spikes. It is a well known phenomenon in fluid mechanics that a jump in the curvature will cause premature flow separation (design rules in [24]). In Wilkinson's experiments $AR = 3$ is too small and $c/H = 0.46$ is too high. The turbulence intensity of his wind tunnel is unknown. The disadvantages of his mean line $a = 0.8$ were already discussed in chapter 3.2.

High quality experimental results are those reported by Bruining [12]. The parameters are listed in chapter 2.2. The round mast has a $D/c = 6.7\%$. His model is only roughly similar to a real sail, but the flow has all the necessary features that are needed to test the prediction code. The wind tunnel had a very low turbulence of 0.02% and the Reynolds-number was as low as 100 000. The XFOIL-predictions display a hysteresis under such conditions. If the angle of attack is reduced in small steps from large to small values, the flow remains separated and the lift coefficient is low. In the opposite direction, the flow remains attached and the lift coefficient is high. Figure 11 depicts all the results from both directions. All the crosses represent converged solutions for the same set of parameters and free transition. At $\alpha = 12°$ the extreme XFOIL-predictions differ by a factor of almost 2. The corresponding diagrams for the pressure coefficients are shown in figure 12. In 12a the transition occurs at

x/c = 0.45. The laminar separation bubble is so long, that the flow cannot fully reattach and remains separated on the rear part of the foil. The lift is low. In 12b the transition occurs at *x/c* = 0.27, the flow reattaches and stays attached until the trailing edge, where a Cp of zero is reached. As a result the lift is high. The experimental value lies in between these extremes. A run of XFOIL with a fixed transition point of *x/c* = 0.386 matches the experimental value at 12°.

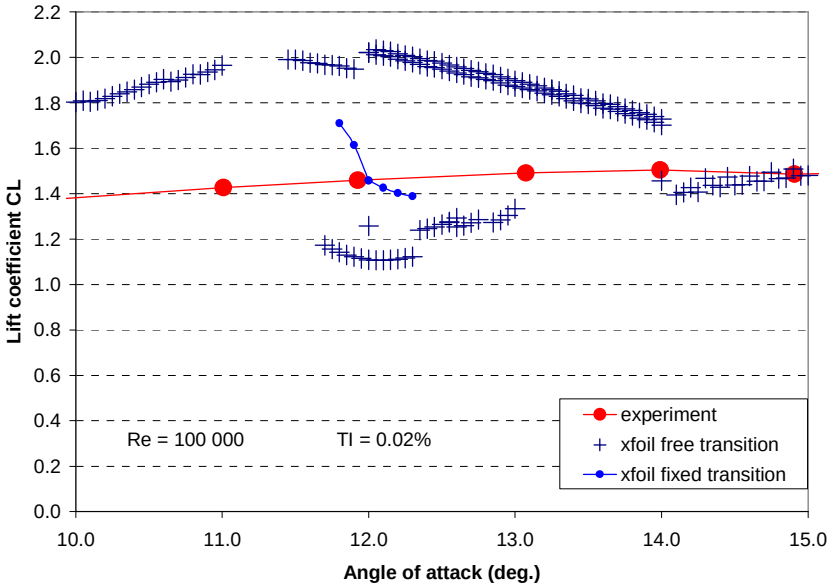

Figure 11. Bruinings test results and XFOIL predictions

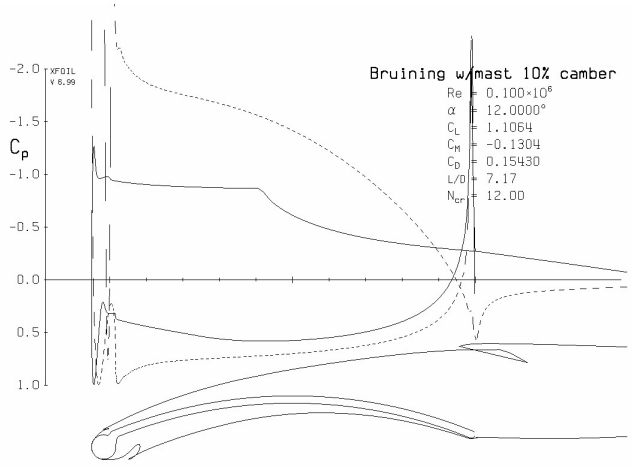

Figure 12a. XFOIL prediction starting at high *α*

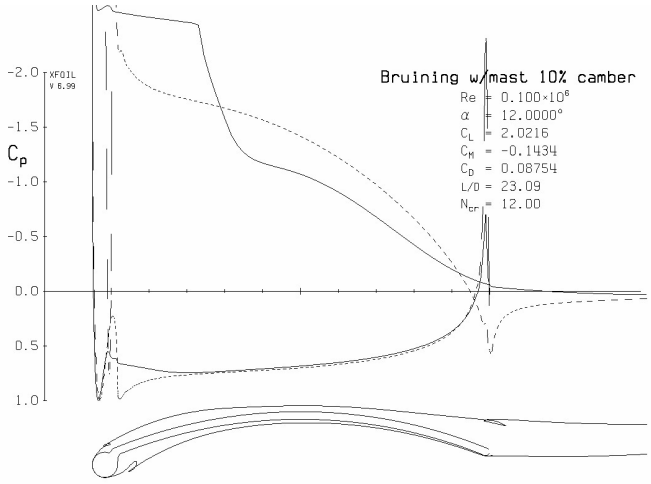

Figure 12b. XFOIL prediction starting at low *α*

The curve for the XFOIL-predictions with this fixed transition point is also depicted in figure 11. One can assume that all values between the extreme predictions are also possible outcomes in the wind tunnel. The actual experimental value depends on uncontrolled parameters like the surface roughness, the 3-D influence of the side walls, any anisotropy of the turbulence, acoustic disturbances and the direction of the variation of *α*. Since the real sail is operated in a highly turbulent flow with bypass transition, the XFOIL-prediction with the shortest transition length, attached flow and high lift will most likely be closer to reality than any experiment in a wind tunnel. This is a general phenomenon. Milgram also tested 2D-sails behind a mast [27]. His lift values are lower than XFOIL-predictions for his model, which is a hint for large separation. As already mentioned the aspect ratio of his model is too small and the blockage is too high. He did not publish the *α*-values for his experiments with a mast and the turbulence intensity is unknown. Given the current situation, the only tool that is suited to create the required large database for the aerodynamic characteristics of sail sections with masts is the XFOIL code. The results seem to be plausible but a full validation is currently not possible.

The XFOIL-predictions for the headsail in chapter 3.1 were corrected according to equation 4 to match the experimental values. For sails with a mast the coefficient *A* in equation 4 is zero, because the mast is large

enough to carry the suction force. If the correction for the T.E. separation should also be applied to the sections with a mast is hard to tell. Since no experimental force measurements with sufficient similarity to sails are available for a validation, we can only rely on our experience as sailors. Figure 13a shows the polar curves for the case without correction and 13b with the correction applied to the drag values. The optimal point for a given C_L lies on the envelope. Without the correction the drag coefficient remains at 0.045 and is almost independent of C_L and camber. With the correction the drag increases significantly with camber and lift. Let us assume, the wind increases in strength and the heeling angle of the boat has to be reduced. If 13a depicted the reality, we would reef the mainsail to reduce the sail force, but would keep the camber and the lift coefficient constant, because a change in camber would have practically no influence on the drag coefficient. Instead, we would have the benefit of the reduced lever arm of the aerodynamic center. If figure 13b were true, we would not reef, but flatten the sail and reduce camber and lift coefficient to achieve a smaller sail force. The benefit would be a significantly smaller drag coefficient. Every sailor knows that in this situation the boat will be faster with flattening than with reefing. We must therefore assume that figure 13b is the situation that describes best the reality. In the following chapters the XFOIL-predictions will be used with the correction for the T.E. separation as in equation 4.

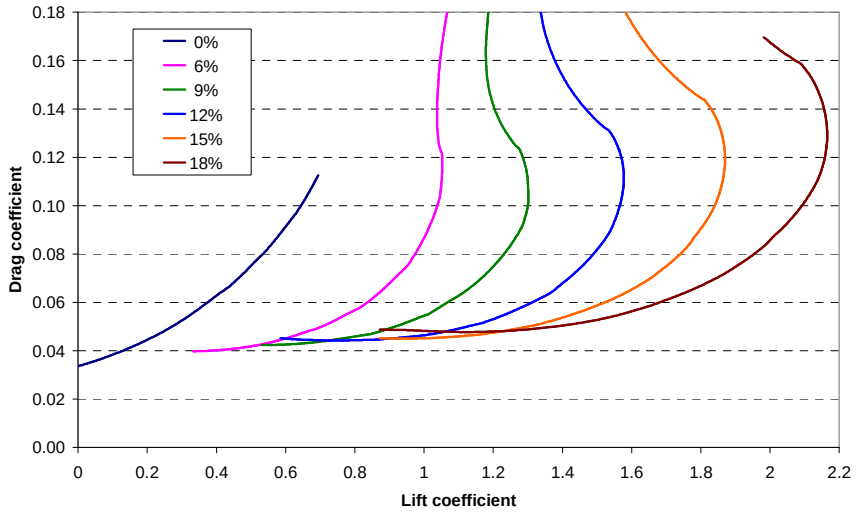

Figure 13a. XFOIL prediction without correction

NACA a = 0.1 modified
f/c = 0% – 18%
t/c = 0.05%
D/c = 10%
γ = 30°
Re = $1 \cdot 10^6$
N_{crit} = 0.5

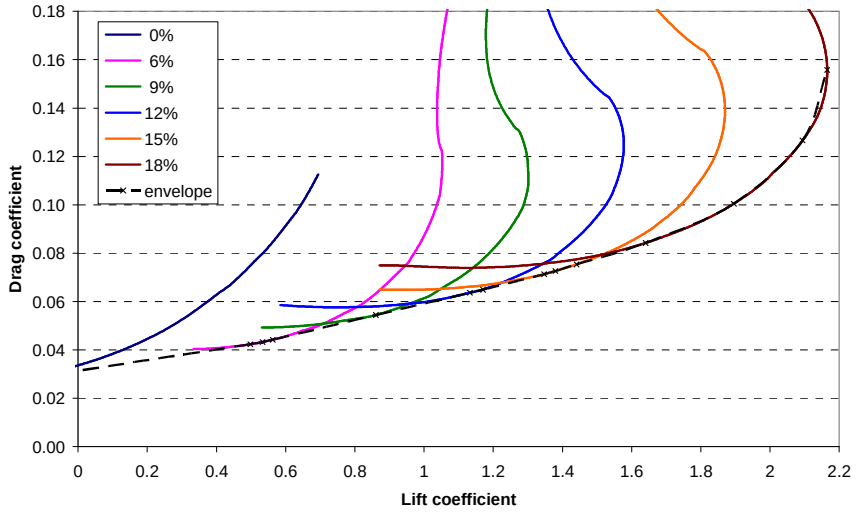

Figure 13b. XFOIL prediction corrected as in eq. 4

4.3 The profile family

The chosen profile family for the mast is the same as for the headsail. Figure 14 shows the XFOIL-predictions for the circular arc profile and the modified NACA profile behind a 10% mast. The NACA sail has lower drag for the same lift. The drag is corrected as in equation 4, but even without this correction, the NACA sail has still an advantage. With the mast influence, it might be possible to find a mean line that is slightly better than the *NACA a = 0.1 modified*, but the uncertainties of the XFOIL-prediction are most likely larger than the differences between "tweaked" mean lines. One might debate an increase of x_f but this will inevitably increase the trailing edge angle β, which will increase the drag. A gentle pressure recovery is even more important with the presence

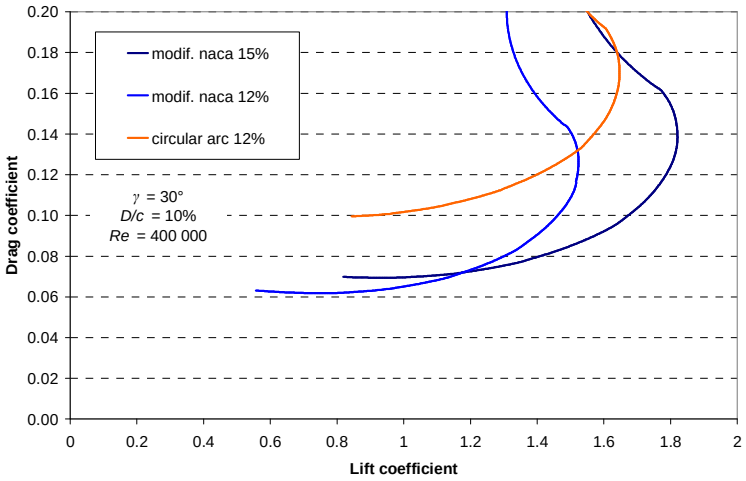

Figure 14. polar curves for sails with mast and different mean lines, XFOIL predictions corrected

N_{crit} = 0.5
x_{tr}/c = 0.01 suction side
x_{tr}/c = 0.04 pressure side

of the mast, because the flow separation is more severe. Figure 15 shows an XFOIL-prediction for a typical trim with a high *L/D*-ratio. The flow is separated behind the mast on both sides of the profile but reattaches at the rear half and stays on both sides attached. A small area behind the mast on the suction side of the model had to be made geometrically smooth, diverging from the true mast/sail contour, otherwise the computation would not converge.

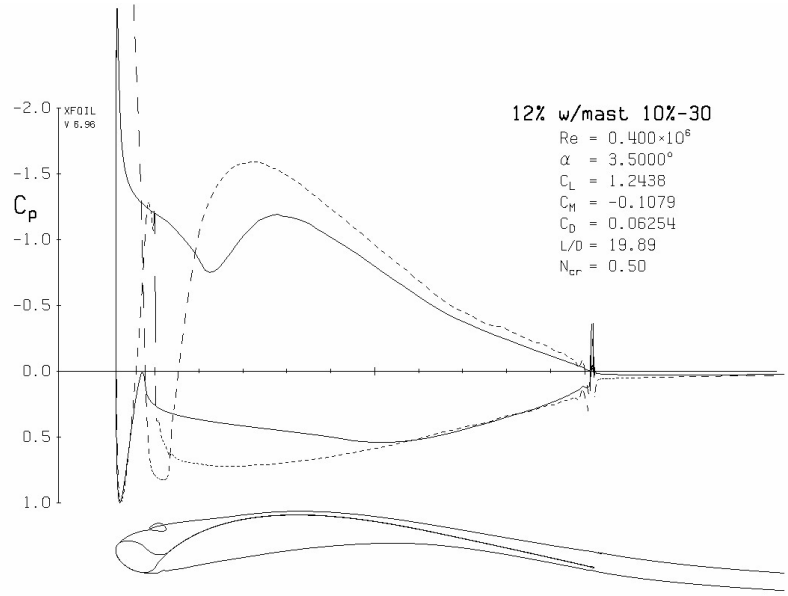

Figure 15. XFOIL prediction with mast *NACA a = 0.1 modified*

f/c = 12%
t/c = 0.05%
D/c = 10%
γ = 30°
α = 3.5°
N_{crit} = 0.5
x_{tr}/c = 0.01 suction side
x_{tr}/c = 0.04 pressure side
Re = 400 000

4.4 Selected results

To create the complete database a large number of different polar curves had to be computed. The independent parameters for the XFOIL-runs were fixed at the following discrete values:

Reynolds-number	$2\cdot10^5$, $4\cdot10^5$, $1\cdot10^6$, $3\cdot10^6$, $9\cdot10^6$
Mast diameter *D/c*	2.7%, 6%, 10%, 20%
Sheeting angle *γ*	5°, 30°, 55°, 80°
camber *f/c*	0%, 6%, 9%, 12%, 15%, 18%
angle of attack *α*	-2° to 20°, densely spaced at 0.05°

For *D/c* = 20% the chord is reduced at the upper part of the sail and *Re* = $9\cdot10^6$ was replaced by $7\cdot10^4$. As described in chapter 3.3, an envelope for the optimal trim follows from the polar curves of varying *α* and camber. These optimal envelopes supply C_D, *α*, *f/c*, and x_{AC} for the given parameters C_L, *Re*, *D/c* and *γ*. The discrete values as are listed above, were chosen in such a way, that all realistic values for full size sailing yachts can be linearly interpolated within the database. An example is depicted in figure 16. For given *Re* and *D/c* the diagram shows the optimal envelopes for discrete values of the sheeting angle *γ*. An intermediate value of *γ* =17° was also tested, because of the large difference between *γ* =5° and *γ* =30°. This test proved that linear interpolation gives

the same results and that the additional workload is not justified. The assumption in [27], that the influence of the sheeting angle on the polar curve is small, is not supported by the XFOIL-computation.

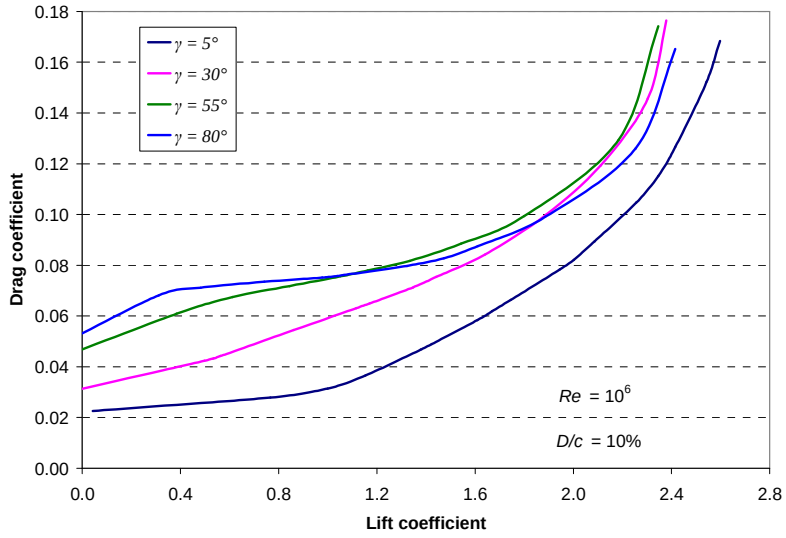

Figure 16. optimal envelopes for varying sheeting angle

The dependence on the Reynolds-number is depicted in figure 17. The drag decreases monotonically with the logarithm of the Reynolds-number.

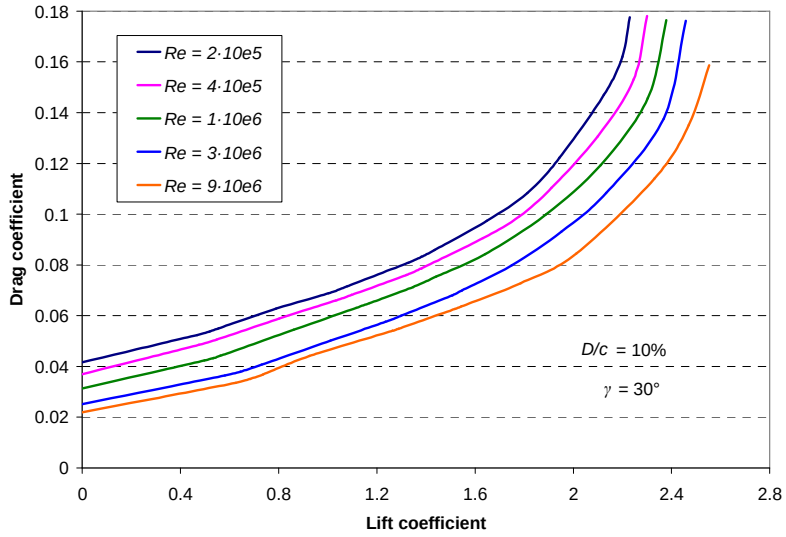

Figure 17. optimal envelopes for varying Reynolds-number

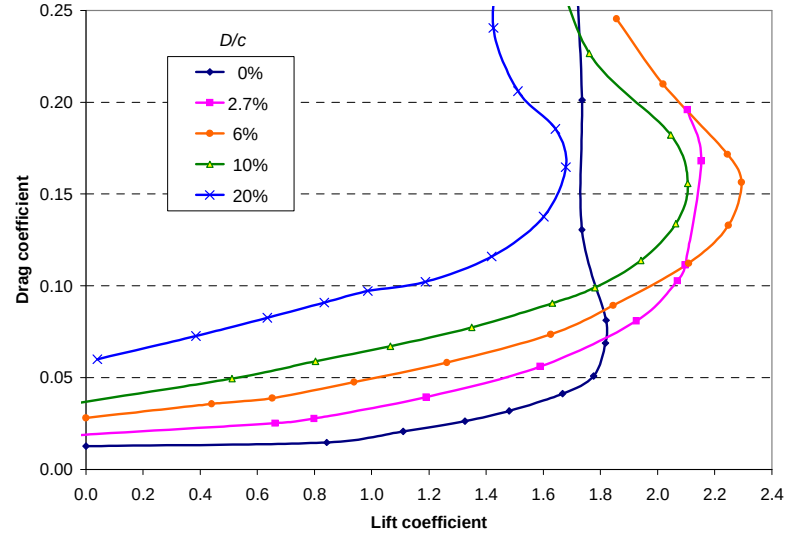

Figure 18. optimal envelopes for varying mast thickness *D/c*

$Re = 4 \cdot 10^5$
$\gamma = 30°$

The influence of the mast is shown in figure 18. It can be seen, that a small mast will increase the achievable maximum lift coefficient, because the mast can carry the suction force at the L.E. With the thin forestay (*D/c* = 0) a suction force is not present. The penalty for the mast is the increased drag. Also visible is the fact, that large *D/c* values at the top of the mast reduce significantly the performance of the sail. A square top mainsail that effectively limits the increase of D/c will preserve the driving force in the sail top.

When investigating large relative mast diameters a phenomenon was encountered. Figure 19 shows, that there is no upper limit for the useful camber. Even a camber of 27% still increases the lift. Since it is not possible to design a sail where the camber can be varied over such a large range, the investigated camber in the computed database was limited to 18%.

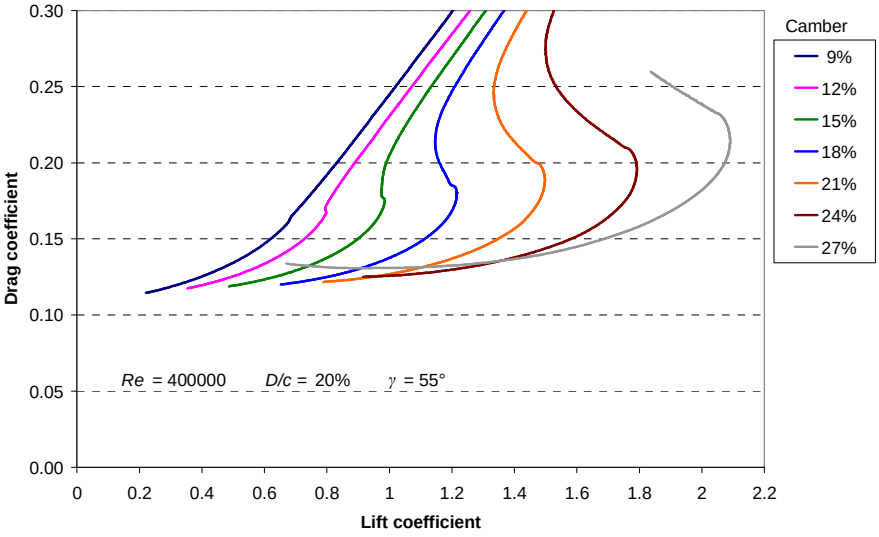

Figure 19. polar curves for 20% mast thickness *D/c*, large sheeting angle and varying camber

4.5 Rotating masts

The disturbance of the flow by the mast and the benefits of a rotating mast are well documented [28]. The XFOIL simulation offers an opportunity to determine polar curves for a fixed and a rotating mast and to compare the results. Especially cruising yachts, which use large mast diameters, travel at low speeds and therefore sail with large sheeting angles would benefit significantly from rotating the mast. Figure 20 compares the polar curves for *D/c* = 10% and different sheeting angles. For a fixed mast the sheeting angle between the chord line and the symmetry-line of the mast increases with the apparent wind angle up to almost 90°. With a rotating mast the angle relative to the chord line can be kept constant at -22°. It is obvious that especially at large apparent wind angles the sail with a rotating mast can produce much larger lift and will have an overall better performance.

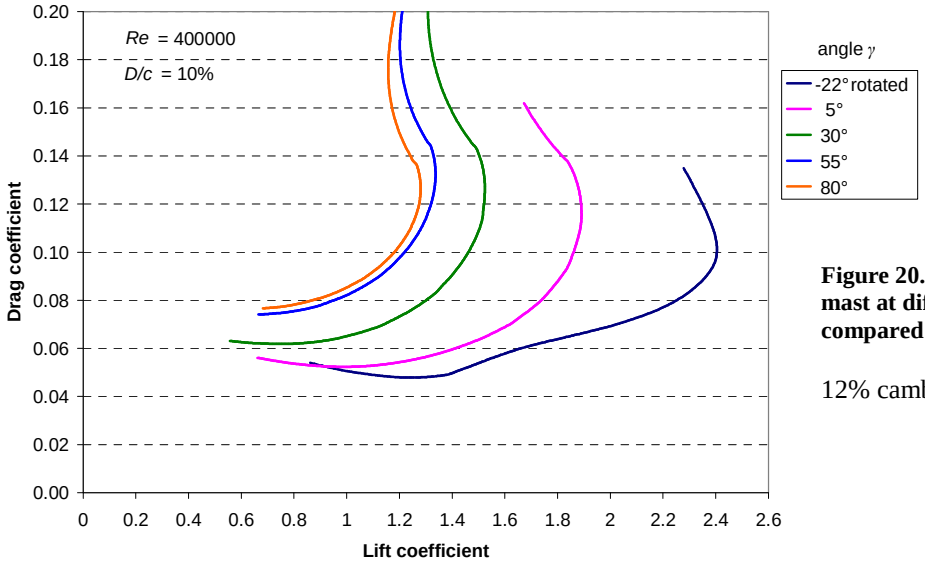

Figure 20. polar curves for 10% fixed mast at different sheeting angles compared to a sail on a rotating mast

12% camber

5 SAIL CHARACTERISTICS FOR REACHING AND RUNNING

5.1 Close reach

In the previous chapters the sail shape was chosen for close-hauled upwind sailing. When bearing away, the side force and hence the heel angle decrease. The sail should now be optimized for maximum lift instead of maximizing the lift/drag ratio. High camber and draft values (x_f/c) near 50% are favorable. The mainsail is normally not changed, only trimmed, by reducing mast bend and luff tension within its limits. The headsail on the contrary can be changed and the shape can be optimized. Figure 21 shows polar curves for headsails with a parabolic shape. The camber is varied between 6% and 31% and the large camber allows α to increase up to 20°. The envelope for the sail shapes with the NACA-mean line is also shown for comparison. It is obvious that for small angles of attack and smaller lift coefficients the NACA-shape is better, because it has a lower drag. The parabola is superior if large lift coefficients are required and drag is not a determining factor.

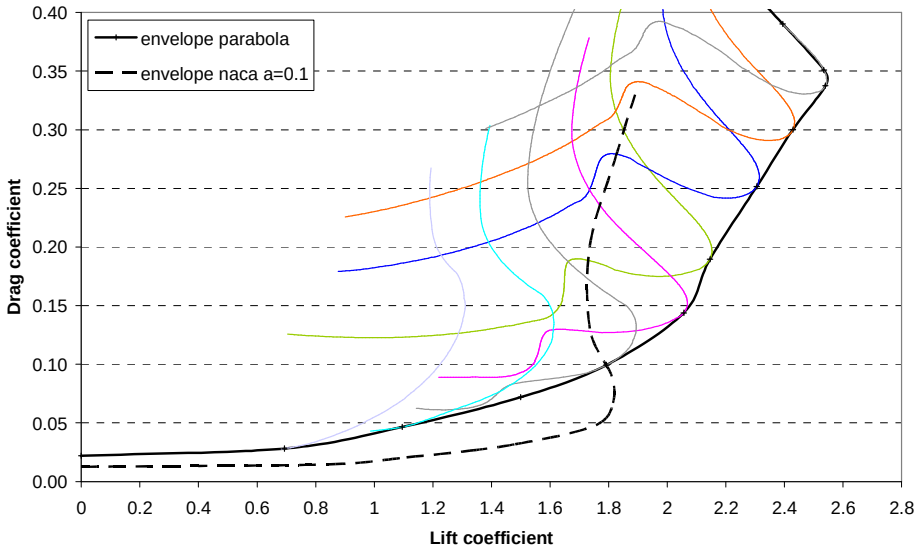

Figure 21. envelope of polar curves for parabolas compared to the modified NACA *a* = 0.1 envelope

Re = 400 000

5.2 Broad reach

The sheeting angle of the headsail is never large enough on a broad reach. To increase the sheeting angle, the clew should be moved outboard as far as possible. On a typical course the headsail would be trimmed as follows:

true wind speed	= 10 kts.	true wind angle	110°
boat speed	= 10 kts.	apparent wind angle	55°
apparent wind speed	= 11.5 kts.	sheeting angle γ	24°

The sheeting angle at deck level can be taken from figure 22 and equation 7. The tangent of the trailing edge angle is proportional to the camber. For a parabola: $\tan(\beta_{TE}) = 4 \cdot f/c$. A large trailing edge angle β_{TE} will increase the sheeting angle and reduce α. Nevertheless, the angle of attack is large. In this case α = AWA – γ = 31°. The flow on the suction side will fully separate at such large angles of attack.

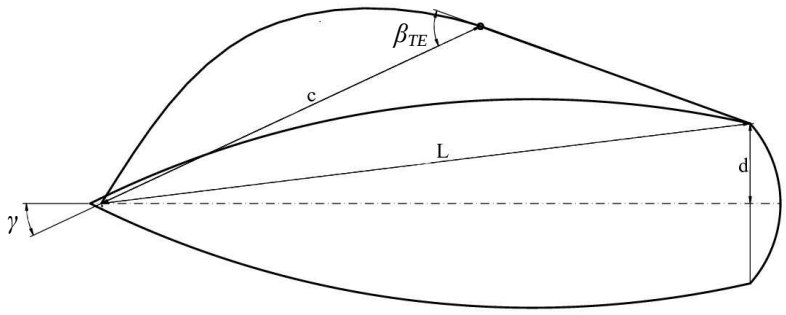

Figure 22. sheeting angle γ projected onto the deck plane

$$\gamma = \arcsin\left(\frac{d}{L}\right) + \arcsin\left(\sin\beta_{TE} \cdot \frac{c}{L} \cdot \left[\sqrt{\frac{L^2}{c^2} - \sin^2\beta_{TE}} - \cos\beta_{TE}\right]\right) \qquad (7)$$

Figure 22 is a projection onto the deck plane. It is not visible that the clew of the sail is significantly above the deck level. It is necessary that the sheet exerts a vertical force component that pulls the clew downwards to avoid the top of the sail twisting open.

Completely separated flows cannot be regarded as two-dimensional any more. Katz & Plotkin [31] show pictures with surface-oil flow patterns for rectangular wings of different aspect ratios. Several stall-cells develop in the span wise direction and the width of these cells is almost independent of the aspect ratio. The problem is therefore three-dimensional and time dependent. Tian et al. [32] demonstrate, that a 2D-simulation (like XFOIL) of an infinite flat plate normal to the free stream overpredicts the drag by a factor of two compared to experimental results and also compared to the 3D-simulation. XFOIL is therefore not a reliable tool any more for such completely separated flows. There are no reports about the aerodynamic characteristics of sails beyond α = 25° in the literature. Available are only investigations of the forces acting on a flat plate. The Rayleigh-Kirchhoff theory gives an estimate of the force on the pressure side of the plate. Hoerner [29] extended this theory and assumed that the pressure on the backside is proportional to the pressure on the front side by a constant factor and that this factor can be taken from the drag value at α = 90°. His theory agrees well with experimental results beyond α = 20°. This method is now likewise applied to a sail. Lindsey [30] measured the drag of a semi tubular cylinder with the concave surface to the wind. The drag coefficient was constant between $Re = 10^4$ and 10^5 and equal to 2.3. The flat plate, the circular arc and the parabola are symmetric around the mid-chord point and the resultant force C_N in fully separated flow is therefore approximately normal to the chord. The coefficients are:

$$C_N = 2.614 \cdot \frac{2 \cdot \pi \cdot \sin\alpha}{4 + \pi \cdot \sin\alpha} \qquad C_L = C_N \cdot \cos\alpha \qquad C_D = C_N \cdot \sin\alpha \tag{8}$$

Figure 23 depicts one of the rare XFOIL predictions that converged and compares it to the estimate of equation 8. When α increases, there is no convergence beyond 24°. Decreasing α, XFOIL converges from 40° downwards and predicts a base pressure that is less negative and gives therefore a lower C_L. We can assume that somewhere between α = 20° and α = 25° the dividing streamline from the separation point at the LE jumps further away from the foil contour, the suction pressure breaks down and the lift coefficient reaches the level of equation 8.

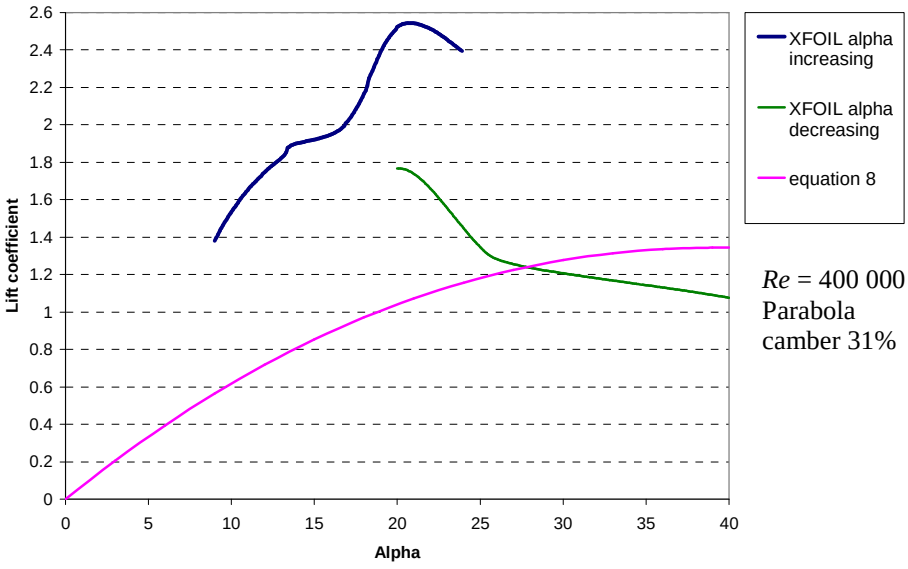

Figure 23. fully separated flow at large AoA

5.3 Running before the wind

Whether running wing and wing or under spinnaker, in both cases the flow over the sails is fully three-dimensional. The streamlines run from a stagnation point in the center of the sail to all sides. There is no resemblance to a wing any more. The best way to calculate the sail forces is the use of global coefficients for the entire sail as described by the ORC [21].

6 CONCLUSION

With the program XFOIL it was possible to create the database of the aerodynamic characteristics for the 2D sail sections over the complete parameter range, with and without a mast. The results are plausible although it is not

possible to truly validate the prediction. This validation would require experimental data that are very difficult to produce. A large wind tunnel for high Reynolds-numbers with high turbulence intensity would be required. The blockage factor should be < 0.3 and the aspect ratio >4. The model would have to be very thin but stiff enough to withstand the wind-forces. At the moment there is nothing better available than what was presented in this paper.

XFOIL was also used to develop an optimized shape of the camber line by modifying the NACA *a*=0.1 line. To build a sail with such a camber, it is necessary to incorporate long battens with a carefully designed bending stiffness. The comment of a sailmaker would be highly interesting.

The created database will be used in a next step to develop a computer program that can calculate the sail forces for an optimized shape. Once this program is available it will be published on www.remmlinger.com.

7 REFERENCES

1. Küchemann, D., "A Simple Method for Calculating the Span and Chordwise Loading on Straight and Swept Wings of any Given Aspect Ratio at Subsonic Speeds", Aeronautical Research Council, R.&M. No. 2935, London, 1956
2. Abbott, I.H., v. Doenhoff, A.E., *Theory of Wing Sections*, New York: Dover, 1959
3. Maughmer, M.D., Coder, J.G., "Comparisons of Theoretical Methods for Predicting Airfoil Aerodynamic Characteristics", Airfoils Incorporated, Subcontract W911W6-07-C-0047, RDECOM, 2010
4. Drela, M., Youngren, H., XFOIL Computer Program, [Online]. Available: http://web.mit.edu/drela/Public/web/xfoil/
5. Weiler, H.S., Burling, R.W., "Direct Measurements of Stress and Spectra of Turbulence in the Boundary Layer Over the Sea", J. Atmospheric Sci., vol. 24, no. 6, pp. 653-664, 1967 https://doi.org/10.1175/1520-0469(1967)024%3C0653:DMOSAS%3E2.0.CO;2
6. Schubauer, G.B., Skramstadt, H.K., "Laminar-boundary-layer oscillations and transition on a flat plate", NACA Rep. 909, 1948
7. Flay, R.G.J., Jackson, P.S., "Flow Simulation for Wind-tunnel Studies of Sail Aerodynamics", *J. Wind Engineering and Industrial Aerodynamics*, vol. 41-44, pp. 2703-2714, 1992
8. Schaffarczyk, A.P., Schwab, D., Breuer, M., "Experimental detection of laminar-turbulent transition on a rotating wind turbine blade in the free atmosphere", *Wind Energy*, https://doi.org/10.1002/we.2001
9. Özçakmak, Madsen, Sørensen, N., Sørensen, J., "Laminar-turbulent transition characteristics of a 3-D wind turbine rotor blade based on experiments and computations", https://doi.org/10.5194/wes-2020-54
10. Flachsbart, O., "Messungen an ebenen und gewölbten Platten", in *Ergebnisse der Aerodynamischen Versuchsanstalt zu Göttingen, IV. Lieferung*, München & Berlin: Oldenbourg, 1932, pp. 96-100
11. Buehring, I., "The Development, Control and Testing of an Aerogenerator", PhD dissertation, Imperial College of Science and Technology, London, 1980
12. Bruining, A., "Aerodynamic Characteristics of a Curved Plate Airfoil Section at Reynolds Numbers 60.000 and 100.000 and Angles of Attack from -10 to +90 Degrees", Report LR-281, Delft University of Technology, 1979
13. Wallis, R.A., "Wind Tunnel Tests on a Series of Circular Arc Plate Aerofoils", Council for Scientific and Industrial Research, Aerodynamics Note 74, Melbourne, 1946
14. Krynytzky, A. "Classical Corrections for Closed Test Sections", in *Wind Tunnel Wall Corrections*, AGARDograph 336, 1998
15. van den Berg, B., "Some Notes on Two-Dimensional High-Lift Tests in Wind-Tunnels", in *Assessment of Lift Augmentation Devices*, AGARD Lecture Series No. 43, 1971
16. de Brederode, V.A., "Three-Dimensional Effects in Nominally Two-Dimensional Flows", PhD dissertation, Imperial College of Science and Technology, London, 1974
17. Souppez, J.R., Arredo-Galeana, Viola, I.M., "Recent Advances in Numerical and Experimental Downwind Sail Aerodynamics", *J. Sailing Technology*, vol. 4, no. 1, pp. 45-65, 2019

18. Milgram, J.H., “Section Data for Thin, Highly Cambered Airfoils in Incompressible Flow”, MIT, Cambridge, Mass., NASA CR-1767, 1971
19. Bot, P., “Force Variations Related to Flow Pattern Changes Around a High-Camber Thin Wing”, *AIAA J*., 2019, https://doi.org/10.2514/1.J058443
20. Newman, B.G., Low, H.T., “Two-dimensional impervious sails: experimental results compared with theory”, *J. Fluid Mech*., vol. 144, pp. 445-462, 1984
21. Offshore Racing Congress VPP documentation 2019
22. Lyon, Broeren, Giguère, Gopalarathnam, Selig, *Summary of Low-Speed Airfoil Data Vol.3*, Virginia Beach: SoarTech Publications, 1997
23. Wilkinson, S., “Partially Separated Flows Around 2D Masts and Sails”, PhD dissertation, University of Southampton, U.K., 1984
24. Chapin, V.G., Jamme, S., Chassaing, P., “Viscous Computational Fluid Dynamics as a Relevant Decision-Making Tool for Mast-Sail Aerodynamics”, *Marine Technology*, vol. 42, no. 1, pp. 1-10, 2005
25. Renzsch, H.F., “Development of a System for the Investigation of Spinnakers Using Fluid Structure Interaction Methods”, PhD dissertation, Delft University of Technology, 2018
26. Kümmel, W., *Technische Strömungsmechanik*, Wiesbaden: Teubner, 2004
27. Milgram, J.H., “Effects of Masts on the Aerodynamics of Sail Sections”, *Marine Technology*, vol. 16, no.1, pp. 35-42, 1978
28. Paton, J.S., Morvan, H.P., “The Effect of Mast Rotation and Shape on the Performance of Sails”, *Int. J. of Maritime Engineering*, A2, no. 103, 2007
29. Hoerner, S.F., *Fluid-Dynamic Lift*, Vancouver, WA, 1985
30. Lindsey, W.F., “Drag of Cylinders of Simple Shapes”, NACA Report No. 619, 1938
31. Katz, J., Plotkin, A., *Low-Speed Aerodynamics*, Cambridge: University Press, 2001
32. Tian, X., Ong, M.C., Yang, J., Myrhaug, D., Chen, G., “Three-Dimensional Effects of The Flow Normal to A Flat Plate at A High Reynolds Number”, *Proc. ASME 2012 31st Int. Conf. Ocean, Offshore & Arctic Engineering*, Rio de Janeiro, 2012